The Astrophysical Journal, 730:30 (8pp), 2011 March 20 doi:10.1088/0004-637X/730/1/30

IN SITU HEATING OF THE 2007 MAY 19 CME EJECTA DETECTED BY *STEREO*/PLASTIC AND *ACE*

Cara E. Rakowski[1], J. Martin Laming[2], and Maxim Lyutikov[3]
[1] Space Science Division, Naval Research Laboratory, Code 7671, Washington, DC 20375, USA
[2] Space Science Division, Naval Research Laboratory, Code 7674L, Washington, DC 20375, USA
[3] Department of Physics, Purdue University, West Lafayette, IN 47907, USA
Received 2010 September 27; accepted 2010 December 28; published 2011 March 1

ABSTRACT

In situ measurements of ion charge states can provide unique insight into the heating and evolution of coronal mass ejections (CMEs) when tested against realistic non-equilibrium ionization modeling. In this work, we investigate the representation of the CME magnetic field as an expanding spheromak configuration, where the plasma heating is prescribed by the choice of anomalous resistivity and the spheromak dynamics. We chose as a test case the 2007 May 19 CME observed by *STEREO* and *ACE*. The spheromak is an appealing physical model, because the location and degree of heating are fixed by the choice of anomalous resistivity and the spheromak expansion rate which we constrain with observations. This model can provide the heating required between $1.1\,R_{\odot}$ and Earth's orbit to produce charge states observed in the CME flux rope. However, this source of heating in the spheromak alone has difficulty accounting for the rapid heating to Fe^{8}–Fe^{11+} at lower heights, as observed in *STEREO* EUVI due to the rapid radiative cooling that occurs at the high densities involved. Episodes of heating and cooling clearly unrelated to spheromak expansion are observed prior to the eruption, and presumably still play a role during the eruption itself. Spheromak heating is also not capable of reproducing the high Fe charge states (Fe^{16+} and higher) seen in situ exterior to the flux rope in this CME. Thus, while the spheromak configuration may be a valid model for the magnetic topology, other means of energization are still required to provide much of the rapid heating observed.

Key words: atomic processes – plasmas – solar wind

Online-only material: color figures

1. INTRODUCTION

The eruption mechanism of coronal mass ejections (CMEs) is currently an extremely active area of research. A variety of mechanisms have been discussed in the literature. Most of these require some form of magnetic reconnection during and after the eruption. The associated thermal heating should be an important diagnostic of the eruptive process, including the eruption dynamics and ejecta geometry, but until now has been relatively unexploited. Such heating gives rise to UV–X-ray emissions during the eruption that can be remotely sensed and also leaves its imprint in the charge states of ions detected in situ near 1 AU, as their ionization state responds to the newly heated plasma. These techniques give complementary insights into the heating and evolution. Spectroscopy is in some sense more direct, being a prompt signature of the eruption, but with existing instrumentation has only been possible relatively close to the solar surface where the signal is strong. Ion charge states, on the other hand, are routinely collected and CMEs, and their constituent parts (forward shock, flux rope, etc.), can easily be identified. Further interpretation of such data requires modeling of the non-equilibrium ionization (NEI) balance as the CME plasma expands outward into the ambient solar wind. In this paper, we explore the consequences of a different source of thermal heating that due to anomalous resistivity within a spheromak solution for the CME geometry as it expands into the solar wind. We compare the predictions of such a model to *STEREO* and *ACE* observations of the 2007 May 19 CME. The structure of the paper is as follows. We describe the status of our understanding of ion charge states observed in CMEs in more detail in Section 2. Section 3 describes the 2007 May 19 CME and some of our motivation for exploring a spheromak model. Section 4 gives the theory of spheromak resistive expansion, with some discussion of just how closely the spheromak model used here may represent a real CME. Section 5 outlines the NEI model incorporating the spheromak resistive heating, and we conclude in Section 6 with a summary of our results in the context of previous research and discuss future modeling improvements.

2. NEI MODELING OF CME CHARGE STATES

Interplanetary CMEs or ICMEs have many well-known signatures. Of these, in situ measurements of ion charge state distributions hold a unique potential for diagnosing the conditions throughout the eruption. The charge states evolve through ionizations and recombinations as a function of temperature and density up to heights of 3–6 solar radii heliocentric distance but are "frozen in" thereafter. Since low-Z ions "freeze-in" at higher densities (i.e., smaller heights or radii) than high-Z ions, they provide complimentary constraints on the temperature evolution.

A number of studies have examined the existing solar wind composition data and made inferences on freeze-in temperatures based on computed ionization distributions appropriate to coronal equilibrium (e.g., Zurbuchen & Richardson 2006; Zurbuchen et al. 2004; Lepri & Zurbuchen 2004; Lepri et al. 2001; Henke et al. 2001; Gloeckler et al. 1998; Henke et al. 1998). However, Rakowski et al. (2007) were the first to conduct time-dependent modeling of the ion charge state distributions of various elements detected in situ in order to draw quantitative conclusions regarding the thermal input and initial conditions in the corona during the CME eruption. Rakowski et al. (2007) modeled the charge states of eight ICMEs from the event list of Lynch et al. (2003), chosen to cover a range of velocities.

Rakowski et al. (2007) considered a simplified geometry for the CME ejecta and parameterized the evolution. The model velocity and expansion were based on the observed phenomenology from plane-of-the-sky events showing that typically CME height–time evolution consists of three phases: initiation, acceleration, and propagation (Zhang et al. 2001, 2004; Zhang & Dere 2006; Sui & Holman 2003; Lin et al. 2005; Sui et al. 2005). Heating of the CME core plasma during the acceleration phase was explored assuming a heating rate for the CME plasma proportional to the rate of kinetic energy increase, i.e., a constant fraction QE/KE during the acceleration up to a final velocity v_f. In five out of eight sample CMEs studied, the dominant Fe charge states were neon-like (16+) or higher, indicating that high temperatures, comparable to flares ($\sim 10^7$K), are involved. Starting the plasma from this temperature and allowing the ions to recombine as they expand could often account for the Fe ionization balance, with peaks around Fe^{16+} and Fe^{8+} (the Ne-like and Ar-like charge states, which have small recombination rates to the next charge states down, hence population "bottlenecks" here). However, the lower-Z elements placed a limit on the maximum starting temperature (at least if assuming ionization equilibrium in the seed plasma). Above $\sim 2.5 \times 10^6$ K, O would have been mainly O^{8+} instead of O^{7+} and O^{6+} as observed and would not recombine significantly during the CME evolution. Evidently, plasma must start out much cooler and be further heated as the CME accelerates. Thermal energy inputs on the order of 2–10 times the kinetic energy were needed in seven out of eight events studied.

Similar conclusions to Rakowski et al. (2007) about the thermal energy input to CMEs have been reached from analysis of ultraviolet spectra taken by *SOHO*/UVCS. Akmal et al. (2001) studied a 480 km s^{-1} CME observed on 1999 April 23 and found a thermal energy comparable to the bulk kinetic energy of the plasma. Ciaravella et al. (2001) give similar results for the 260 km s^{-1} 1997 December 12 CME. More dramatically, Lee et al. (2009) studied the 2001 December 13 event, and using the combination of [O v] density diagnostics and NEI modeling of O vi found that 75% of the magnetic energy must go into heat to match the UVCS observations. Rakowski et al. (2007) found a heat to kinetic energy ratio of at least 6 for the same event.

The motivations behind the current work are twofold. First, to test if our NEI modeling of the charge state distributions can hold up to the scrutiny of additional constraints on the eruption dynamics coming from *STEREO* observations in the 2007 May 19 CME, as well as observations regarding the charge states closer to the Sun. Second, we explore whether a more physically and theoretically specified heating model when incorporated into our non-equilibrium modeling can reproduce the charge states of a real event with reasonable physical parameters.

3. THE 2007 MAY 19 CME

The 2007 May 19 CME studied in this paper is qualitatively different from those CMEs discussed above. As one of the first major CME eruptions in the *STEREO* era the 2007 May 19 event has been intensely studied by multiple authors (Gopalswamy et al. 2009; Veronig et al. 2008; Li et al. 2008; Liu et al. 2008; Kilpua et al. 2009; Liewer et al. 2009; Bone et al. 2009; Kerdraon et al. 2010). It began as a filament eruption from the active region AR10956 and was detected as an ICME by *STEREO B*, *ACE*, and possibly *STEREO A* on 2007 May 22. Multiple heating and cooling episodes were seen in the two days prior to eruption (Liewer et al. 2009; Bone et al. 2009; Li et al. 2008). The total unsigned flux declined 17% in the two days prior to the first eruption (Li et al. 2008). During that time at least four heating (and cooling) events happened which heated the filament to 1 MK or higher (Bone et al. 2009). According to Bone et al. (2009), the formation and merger of the filament which eventually erupted represents 6% of the total unsigned flux change during this two day period.

Our model of the heating during the CME eruption and evolution through interplanetary space will need to match both the charge states seen in the filament during eruption and detected in situ, as well as the density and speed of the ejected material. Liewer et al. (2009) present the *STEREO* EUV images showing the heating of the filament in the hours and minutes immediately preceding the eruption. Hot spots are seen in the EUVI 171 Å filter (mainly Fe ix and xii) at heights near 1.07 $R_\odot$. The magnetic cloud is determined to have mainly interacted with *STEREO B*, which penetrated the center during most of May 22 (DoY 142), while *STEREO A* only passed through the magnetic cloud periphery (Kilpua et al. 2009). The in situ Fe charge states seen with PLASTIC on *STEREO B* and *A* are shown in Figure 1.[4] Charge state data from *ACE* for multiple ions are shown in Figure 2. The highest Fe charge states, Fe^{14+} and Fe^{15+}, are only seen in *ACE* and *STEREO A* which were not centrally located in the event, but rather on its flanks. Furthermore, the appearance of the highest charge states is after the cloud passage as defined in Liu et al. (2008).

The shock front around the 2007 May 19 CME launched at 958 km s^{-1}, the average speed in transit to 1 AU was around 700 km s^{-1} and the speed of the MC as it passed the *STEREO B* spacecraft was 482 km s^{-1} (Kilpua et al. 2009). The filament that erupted from the active region at about the same time only rose at an average speed of 103 km s^{-1} (Liewer et al. 2009), but it could have been dragged out by the CME and the fast solar wind to reach a similar coasting velocity as the ICME. It had no distinct initiation or acceleration phase, and clearly does not fit within the phenomenology described above and in Rakowski et al. (2007), which leads us to consider a spheromak model for the CME evolution.

4. RESISTIVE SPHEROMAK MODEL OF CMEs

4.1. Spheromak Field Configurations

Spheromaks are well-known force-free configurations of plasma satisfying condition $\nabla \times \mathbf{B} = \alpha \mathbf{B}$ with spatially constant α. They are solutions of the Grad–Shafranov equation in spherical coordinates with the poloidal current being a linear function of the flux (Chandrasekhar & Kendall 1957). The basic spheromak solution is

$$\begin{aligned} B_r &= 2B_0 \frac{j_1(\alpha r)}{\alpha r}\cos\theta \\ B_\theta &= -B_0 \frac{j_1(\alpha r) + \alpha r j_1'(\alpha r)}{\alpha r}\sin\theta \\ B_\phi &= B_0 j_1(\alpha r)\sin\theta, \end{aligned} \tag{1}$$

where the spherical Bessel function j_1 can be expressed in terms of elementary functions, $j_1(x) = \sin x/x^2 - \cos x/x$. The parameter α is related to the size of the spheromak R, defined by the surface where radial magnetic field is zero, given by the solution of $j_1 = 0$; $R = C_\alpha/\alpha$ with $C_\alpha = 4.49$.

The spheromak model of CME topology is an attractive alternative to the usual flux rope model. It is self-contained with

[4] Links to the level 2 data are available at http://fiji.sr.unh.edu/.

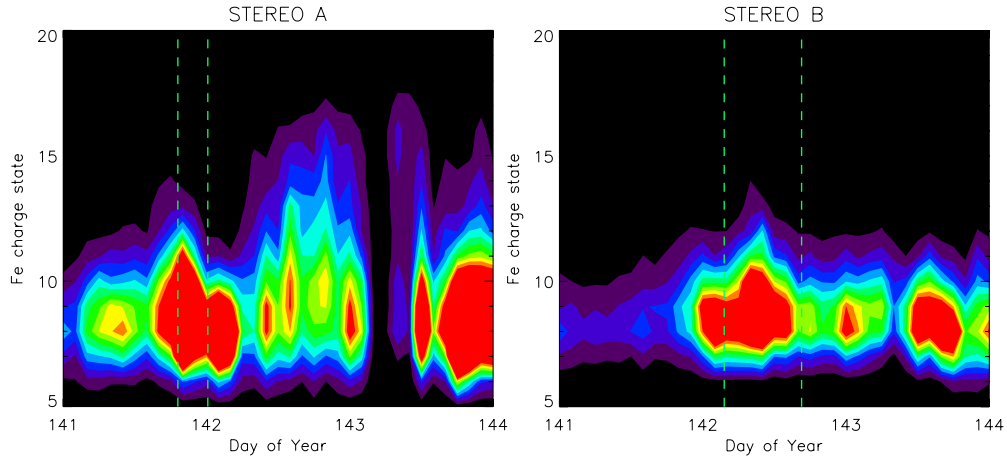

Figure 1. Fe charge state distributions detected by *STEREO A* and *B* during the 2007 May 19 CME passage. Highest Fe charge states are detected by *STEREO A*, though the magnetic cloud is more clearly detected in *STEREO B*. Magnetic field and other data indicate cloud passage between 3:36 hr and 16:34 hr on day 142 (May 22) for *STEREO B* and May 21 19:12 until May 22 00:14 for *STEREO A* (Liu et al. 2008). The dashed vertical lines show the temporal extent of the magnetic cloud (or flux rope) in this event.

(A color version of this figure is available in the online journal.)

no unknown "length of flux rope" parameter to maintain connectivity to the Sun and the heating within it is mathematically specified once the anomalous resistivity is chosen. The torus structure, seen on edge, may even resemble the filament shape in some CMEs (Kataoka et al. 2009). Previously, Lyutikov & Gourgouliatos (2010) found ideal self-similar solutions for expanding spheromak, with electric fields

$$\mathbf{E} = \frac{r}{c}\frac{\dot{\alpha}}{\alpha}\mathbf{e}_r \times \mathbf{B} \tag{2}$$

(dot denotes differentiation with respect to time) and the corresponding non-radial velocity field

$$\mathbf{v} = \frac{\mathbf{B}(\mathbf{B}\cdot\mathbf{e}_r) - \mathbf{e}_r B^2}{B^2} r\partial_t \ln\alpha. \tag{3}$$

In this section, we discuss continuous heating of an expanding spheromak, generalizing the previous analysis to non-ideal self-similar expansion with $\mathbf{E}\cdot\mathbf{B} \neq 0$.

Physically, the parallel component of the electric field should be related to the current density through Ohm's law. Formally, the procedure described below breaks down the assumption of self-similarity, since the value of the parallel electric field component is not linearly proportional to the current density. Still, we assume that resistivity plays a subdominant role, so that the expansion remains approximately self-similar. In other words, we assume that resistivity leads to small deviation from the ideal self-similar expansion. The resulting dynamics remain self-similar, by assumption, but are a little different from the ideal case. We are interested not in the detailed properties of local resistive heating, but in general scaling relations. As we show below, the requirement that an expanding CME dissipates some of its initial energy in the form of heat, detectable by its effect on element charge states by the time it reaches Earth's orbit, can be used to estimate the anomalous resistivity.

Expressing electric field in radiation gauge $\mathbf{E} = -\partial_t\mathbf{A}/c$, where $\mathbf{A}$ is vector potential, we find from the force-free condition

$$\partial_r(rA_\theta) - \partial_\theta A_r = \alpha r A_\phi. \tag{4}$$

This equation highlights two important points. First, it shows how the time dependences of the poloidal components of the vector potential are related to the toroidal components, $A_\theta, A_r \propto \alpha(t)A_\phi$ (this is related to the conservation of poloidal

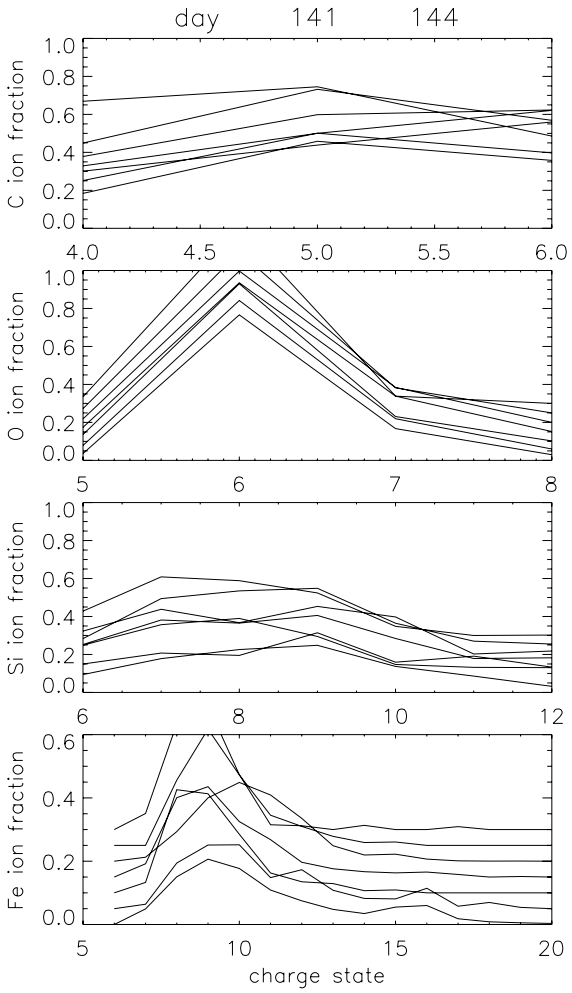

Figure 2. *ACE* charge state data for C, O, Si, and Fe in 8 hr bins. Earliest times have been offset upward for display purposes. The highest Fe charge states only appear starting in Day 143 after the passage of the interior of the magnetic cloud. Liu et al. (2008) report the ICME passages through *ACE* as 21 May 22:19 to 22 May 12:43.

and toroidal fluxes). Second, we get one equation for the two functions A_r, A_θ. Since spheromak solutions are linear, a general solution is a linear combination of the two solutions. The two particular solutions, which in a static case correspond to two equivalent choices of the poloidal components of vector potential, in a time varying case correspond to different physical processes. Accordingly, there are two types of solutions, corresponding to two choices of vector potential in Equation (4), $A_r \neq 0$ and $A_\theta \neq 0$. We consider them in turn.

4.2. Resistive Expansion of First Type

Let us assume that B_ϕ scale with time as an arbitrary function of the expansion parameter, $B_\phi \propto f(\alpha/\alpha_0)$. The first type of solutions has $A_r = 0$ and, from Equation (1),

$$A_\theta = -B_0 f(\alpha/\alpha_0)\frac{\left(\sin(\alpha r) - \int^{\alpha r}\frac{\sin z}{z}dz\right)}{\alpha^2 r}\sin\theta. \quad (5)$$

The first electromagnetic invariant $\mathbf{E}\cdot\mathbf{B} \propto \left(\alpha\dot{f} - 2\dot{\alpha}f\right)$. Thus, if $f = (\alpha/\alpha_0)^2$ the flow is ideal, consistent with the scaling chosen in Lyutikov & Gourgouliatos (2010). More generally, if we allow $f = (\alpha/\alpha_0)^{2+m}$, we find the parallel electric field

$$E^2_{\parallel,1} = m^2 B_0^2(\alpha/\alpha_0)^{2m}\frac{\dot{\alpha}^2\sin^4\theta}{\alpha_0^4 c^2}F_1(r\alpha,\theta), \quad (6)$$

where $F_1(r\alpha,\theta)$ is a lengthy function not given explicitly here. The case of $m = 0$ corresponds to ideal expansion. Since we expect that reconnection eliminates magnetic flux, physically realizable solutions correspond to $m > 0$. Magnetic flux decreases as $\alpha^m \propto R^{-m}$.

4.3. Resistive Expansion of Second Type

The second type of dissipative expansion corresponds to $A_\theta = 0$ and

$$A_r = B_0 r f(\alpha/\alpha_0) j_1 \cos\theta. \quad (7)$$

The parallel electric field in this case

$$E^2_{\parallel,2} = B_0^2(\alpha/\alpha_0)^{2(m-1)}\frac{\dot{\alpha}^2}{\alpha_0^4 c^2}F_2(r\alpha,\theta). \quad (8)$$

For this solution the resulting electric field has a component along magnetic field for any m. The resistive effects in these solutions are induced exclusively by spheromak expansion. Note that this is different from resistive decay of a stationary spheromak, which proceeds homologously. Thus, expansion of the spheromak generally leads to appearances of parallel electric fields and associated dissipation, which can proceed much faster than resistive decay of stationary spheromaks.

4.4. Expansion-driven Dissipation

Let us concentrate on the resistive expansion of first type, which produces equatorial dissipation concentrated in the flux rope, as in the CME observations we attempt to model. The dynamical models described above relate the resistivity to the overall dynamics. The volume integral over $E^2_\parallel$ (see Equation (6)) is

$$\int E^2_\parallel dV = 0.033 m^2 B_0^2 R_0^3 \frac{v^2}{c^2}\left(\frac{R_0}{R}\right)^{2m+1}, \quad (9)$$

which leads to the dissipation rate

$$\dot{\epsilon} = \int \frac{E^2_\parallel}{\eta}dV = 0.033 m B_0^2 R_0^3\left(\frac{R_0}{R}\right)^{2m+1}\frac{v}{R}, \quad (10)$$

with the identification of the resistivity $\eta = mRv/c^2$. This is justified by integrating the energy dissipation rate above between R_0 and R to give a total dissipated energy

$$\int_{R_0}^{R}\frac{\dot{\epsilon}}{v}dr = 0.033\frac{m}{2\eta}\frac{B_0^2}{c^2}v R_0^4\left(1-\left(\frac{R_0}{R}\right)^{2m}\right) \simeq 0.033\frac{m}{2\eta}\frac{B_0^2}{c^2}v R_0^4 \times 2m\ln\left(\frac{R}{R_0}\right), \quad (11)$$

where the last step assumes $(R - R_0)/R_0 \ll 1$. With total spheromak (magnetic) energy $U = 1.57\times10^{-2}B_0^2R_0^4/R \times (R_0/R)^{2m}$, the difference in energy between R_0 and R is $\delta U = U(R_0)(1-(R_0/R)^{2m+1})$, of which a fraction $2m/(2m+1)$ is dissipated. Writing

$$\delta U \simeq 2mU(R_0)\ln\left(\frac{R}{R_0}\right) = 0.033 B_0^2 R_0^3\ln\left(\frac{R}{R_0}\right) \quad (12)$$

and equating with $\int_{R_0}^{R}\frac{\dot{\epsilon}}{v}dr$ in Equation (11) yields $\eta = mR_0v/c^2$. This is derived assuming an infinitesimal expansion. The generalization to arbitrary expansions gives

$$\eta \simeq mRv/c^2. \quad (13)$$

In the second case the dissipation rate

$$\int \mathbf{E}\cdot\mathbf{J}dV = B_0^2R_0^3\left(\frac{R_0}{R}\right)^{2(m+1)}V F_2(m), \quad (14)$$

where $F_2(m) \approx 0.033m - 5\times10^{-4}$, very similar to the first case when integrated over the spheromak volume. The distribution of the heating is different in the two cases, as illustrated in Figure 3. The amount of energy available for heating therefore depends on the value of the anomalous resistivity and varies with position in the spheromak about an average value. The distribution of volumetric heating rates for the first type of dissipative solutions (of most interest here; see below) is given in Figure 4.

To what extent can a spheromak approximate a real CME? Flux rope structures, similar to the equatorial portion of a spheromak, are frequently observed in situ, through the rotation of the magnetic field as the spacecraft penetrates the CME plasma. The precise origin of the flux rope is not clear. Many authors assume that such a structure emerges fully formed from the photosphere (e.g., Fan & Gibson 2004; Magara & Longcope 2003). Alternatively in the breakout (e.g., Antiochos et al. 1999; Lynch et al. 2004), tether-cutting (e.g., Moore et al. 2001), or flux cancellation (e.g., Linker et al. 2003) models, the flux rope forms as the CME erupts by the reconnection along an arcade of magnetic loops. In such a case, the ends of the flux rope remain attached to the Sun during the eruption. A spheromak however is a self-contained magnetic field configuration supported by internal currents, with no external attachment, and presumably if appropriate, must emerge fully formed from beneath the solar photosphere.

In general, the models in which a flux rope forms by reconnection predict an acceleration phase at the onset of flare

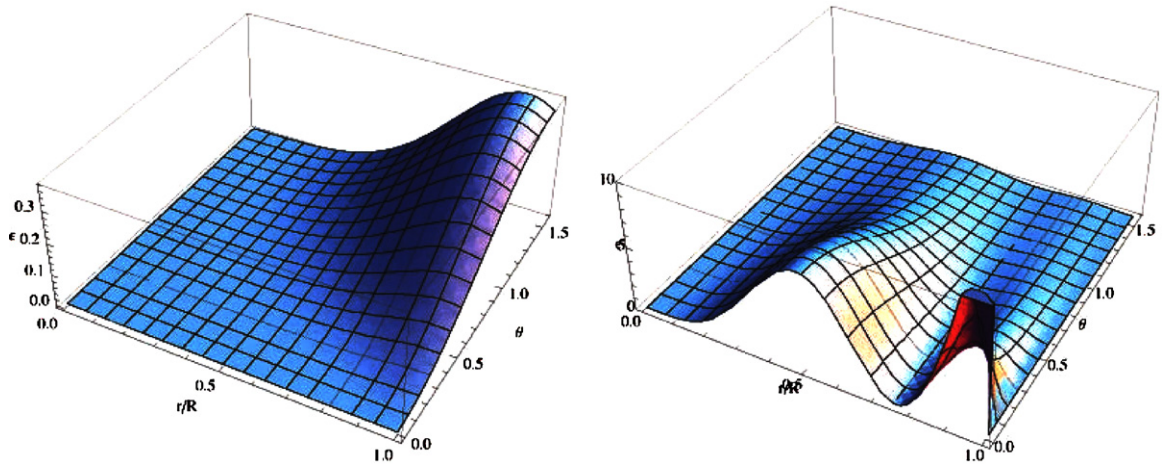

Figure 3. Normalized dissipation rate ϵ as function of radial distance $r/R(t)$ and polar angle θ for two self-similar dissipative structures, $m = 1$. Left panel: solutions (5) and (6). Right panel: solutions (7) and (8).

(A color version of this figure is available in the online journal.)

reconnection. By contrast, the 2007 May 19 CME appears to have moved out from very low down at almost constant speed. There is no obvious feature in its height–time plot that would correspond to the onset of an acceleration phase coupled with reconnection to form a flux rope, suggesting that the observed flux rope must have formed much lower down. Thus, its observed trajectory suggests that a spheromak might be a more appropriate description here, than it would have been for other CMEs considered previously in Rakowski et al. (2007). Nakagawa & Matsuoka (2010) find a similar trajectory for the magnetic cloud observed by *ACE* and Nozomi on 1999 April 16–18. They also conclude that the magnetic cloud is better fitted by a toroidal, as opposed to cylindrical, flux rope, though the model fitted is still approximate. Both flux ropes and spheromaks conserve helicity as they expand, and to do so must decrease their magnetic energy, a part of which can end up dissipated as heat. Kumar & Rust (1996) consider an expanding flux rope and find temperatures reaching $(1–2)\times10^6$ K. We apply similar ideas, derived within the context of a spheromak, to the 2007 May 19 CME. We assume that the expansion velocity of the spheromak entering the expression for the heating is given by the observed motion of the CME.

5. SPHEROMAK NON-EQUILIBRIUM IONIZATION MODEL OF THE 2007 MAY 19 CME

As in Rakowski et al. (2007), we modeled the charge states within the CME ejecta for a variety of ions using an adaptation of the BLASPHEMER (BLASt Propagation in Highly EMitting EnviRonment) code (Laming & Grun 2002, 2003; Laming & Hwang 2003), which follows the time-dependent ionization balance and temperatures of a Lagrangian plasma parcel as it expands in the solar wind. The fundamental equations are outlined below. Further details of the ionization and recombination calculation can be found in Rakowski et al. (2007) and references therein.

The density n_{iq} of ions of element i with charge q is given by

$$\frac{dn_{iq}}{dt} = n_e(C_{\mathrm{ion},q-1}n_{iq-1} - C_{\mathrm{ion},q}n_{iq}) + n_e(C_{\mathrm{rr},q+1} + C_{\mathrm{dr},q+1})n_{iq+1} - n_e(C_{\mathrm{rr},q} + C_{\mathrm{dr},q})n_{iq}, \quad (15)$$

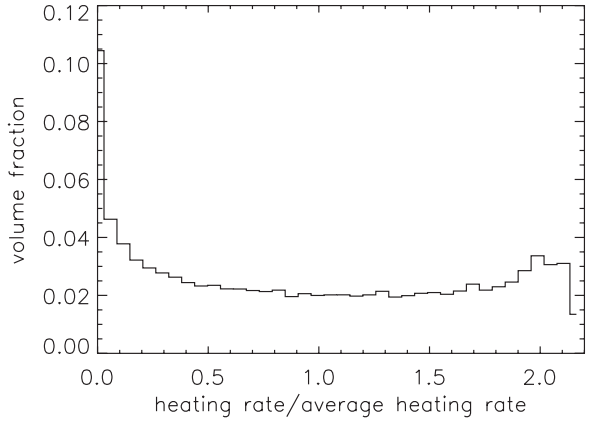

Figure 4. Distribution of volumetric heating rates in the spheromak model of the first type, solutions (5) and (6), in terms of the average heating rate over the whole volume.

where $C_{\mathrm{ion},q}$, $C_{\mathrm{rr},q}$, and $C_{\mathrm{dr},q}$ are the rates for electron impact ionization, radiative recombination, and dielectronic recombination, respectively, out of the charge state q. These rates are the same as those used in the recent ionization balance calculations of Bryans et al. (2006), with more recent updates given in Rakowski et al. (2007). The electron density n_e is determined from the condition that the plasma be electrically neutral. The ion and electron temperatures, T_{iq} and T_e, are coupled by Coulomb collisions by

$$\frac{dT_{iq}}{dt} = -0.13n_e\frac{(T_{iq} - T_e)}{M_{iq}T_e^{3/2}}\frac{q^3n_{iq}/(q+1)}{\left(\sum_{iq} n_{iq}\right)}\left(\frac{\ln\Lambda}{37}\right) \quad (16)$$

and

$$\frac{dT_e}{dt} = \frac{0.13n_e}{T_e^{3/2}}\sum_{iq}\frac{(T_{iq} - T_e)}{M_{iq}}\frac{q^2n_{iq}/(q+1)}{\left(\sum_{iq} n_{iq}\right)}\left(\frac{\ln\Lambda}{37}\right) - \frac{T_e}{n_e}\left(\frac{dn_e}{dt}\right)_{\mathrm{ion}} - \frac{2}{3n_ek_\mathrm{B}}\frac{dQ}{dt} + \frac{\dot{\epsilon}}{1.5n_ek_\mathrm{B}}. \quad (17)$$

Here, M_{iq} is the atomic mass of the ions of element i and charge q in the plasma, and $\ln\Lambda \simeq 28$ is the Coulomb logarithm. The term in dQ/dT represents plasma energy losses due to ionization

and radiation. Radiation losses can be taken from Summers & McWhirter (1979). In a CME from a filament eruption the densities and temperatures are such that radiative losses can be important, unlike most applications in the solar wind where they are generally negligible. The term $-(T_e/n_e)(dn_e/dt)_{\rm ion}$ gives the reduction in electron temperature when the electron density increases due to ionization. Recombinations, which reduce the electron density, do not result in an increase in the electron temperature in low-density plasmas, since the energy of the recombined electron is radiated away (in either radiative or dielectronic recombination), rather than being shared with the other plasma electrons as would be the case for three-body recombination in dense plasmas. We include the last electron heating term to model the Ohmic dissipation given by Equation (10) for the heating in the spheromak.

In addition to ionization and recombination there is also the geometry to consider in the density and temperature evolution. For lack of a better motivated profile, we chose a uniform initial density and temperature, exploding from an initial radius of $(z_0 - 1)$ where z_o is the starting height from the center of the Sun in solar radii. Thus, the underlying density evolution for adiabatic expansion goes as $[(z - 1)/(z_0 - 1)]^2$, which goes over to $(z/z_0)^2$ as $z \gg z_0$ and the CME expansion more closely follows that of the ambient solar wind.

There are two questions we are trying to answer with our simulations. First, how well can a spheromak solution explain the charge states seen in the 2007 May 19 event? To this end, two sets of models were explored. In model 1, we attempted to match both the filament heating and the ICME charge states using only the heating due to anomalous resistivity in the spheromak. In model 2, we allowed the plasma to already have been heated during the eruption to temperatures that would explain the EUVI observations, but then followed the subsequent heating in the spheromak. Second, given that fast CMEs, particularly at solar maximum, often show Fe charge states as high as Fe^{17+} in situ, what are the highest Fe charge states obtainable by anomalous resistive heating in a spheromak model? In other words, how general could such a model be?

The baseline model 1 starts the plasma at a temperature of 10^4 K, a density of 10^{10} cm^{-3}, and a velocity of 10 km s^{-1} accelerating to 500 km s^{-1}. These were chosen as appropriate temperatures and densities for cool filament material, and the evolution is consistent with the final density seen in situ. We initially explored the effect on the final charge states of changing the anomalous resistivity, and thus the amount of magnetic flux dissipation, through the parameter m. We assumed heating at the average rate for the spheromak volume. Values of m of 0.01 and below leave the charge states essentially unaffected by the spheromak heating. (The charge states still evolve with the adiabatic expansion which changes the temperature and density as the CME erupts.) At m values between 1.5 and 2 one reaches the limit of diminishing returns whereby increasing m does not result in higher charge states, due to the factor $(R_0/R)^{2m}$ in Equation (10). This corresponds to an anomalous resistivity between 8×10^{-5} s and 10^{-4} s, as much as 10^{11} times the *Spitzer* value, with a maximum Fe charge state of Fe^{13+}. We note that increasing the final velocity or the acceleration rate does not substantially change this limit. A more dramatic spheromak expansion starting from a smaller sphere does heat the material faster, but it also reduces the density too quickly such that (1) the final densities are substantially lower than seen in situ and (2) ionization declines such that the highest charge states are not produced. Thus, we conclude that the high charge states over Fe^{13+} in fast CMEs cannot be reproduced purely with the spheromak solution and anomalous resistivity. This leaves the question of how well the spheromak can explain this particular 2007 May 19 CME.

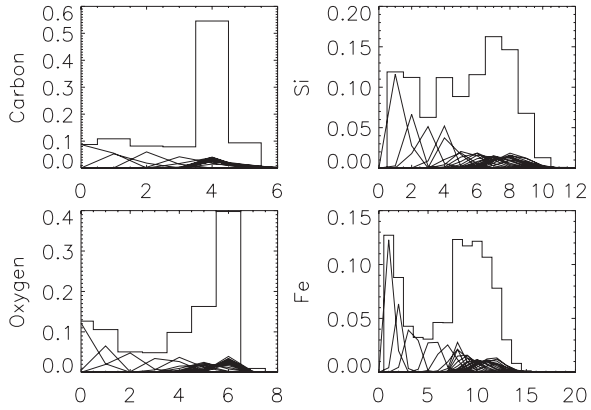

Figure 5. Final charge state distributions of C, O, Si, and Fe for model 1. The individual lines show the contributions from regions within the spheromak with different heating rates. The histograms show the cumulative charge distribution assuming a volume-weighted summation.

We choose $m = 0.75$ and compute ion charge states averaged over the whole spheromak assuming the distribution of heating rates in Figure 3. Since the 2007 May 22 CME flux rope does not exhibit Fe more ionized than Fe^{13+}, its highest charge states can be explained with the baseline model 1 and an average $m = 0.75$. The overall weighted charge states of this model are shown in Figure 5. There are two obvious discrepancies between in situ observations and the Fe charge states modeled here. First, there are too many low charge states from the unheated portion of the spheromak. This is not a major concern as it is possible that that portion of the spheromak is simply not filled with plasma. Second, carbon charge states seem to indicate that the plasma started hotter than in these simulations.

Additionally, one can consider whether the spheromak heating could explain the EUV observations of the filament around launch. Figure 6 shows the early evolution of the charge states corresponding to the average heating rate near the Sun in the baseline model 1 with $m = 0.75$. This started with the plasma at 1.1 $R_\odot$, above the heights of 1.07 $R_\odot$ where Liewer et al. (2009) first see Fe IX and Fe XII emission. Starting simulations below this height, with a density that evolves to become the observed density in situ at Earth's orbit, lead to strong radiative cooling that keeps the electron temperature below $\sim 10^4$ K until a radius of 1.1 $R_\odot$ is reached, whereupon the density is sufficiently reduced to lengthen the radiative cooling time. Hence the heating observed by Liewer et al. (2009), beginning before the actual eruption began, must have had a different origin.

Testing models that started at lower heights, we found that indeed Fe IX and even Fe XII could be produced within a short distance of launch. We did not use these for our in situ modeling because for reasonable starting filament densities the final density due to the rapid expansion was too low. Overall, we conclude that while reproducing the EUV observations may be possible within a spheromak context, given the sequence of heating and cooling of the filament leading up the event as described by Bone et al. (2009), it is also plausible, and probably more likely, that whatever mechanism was heating the filament pre-eruption was responsible for the filament heating during the eruption.

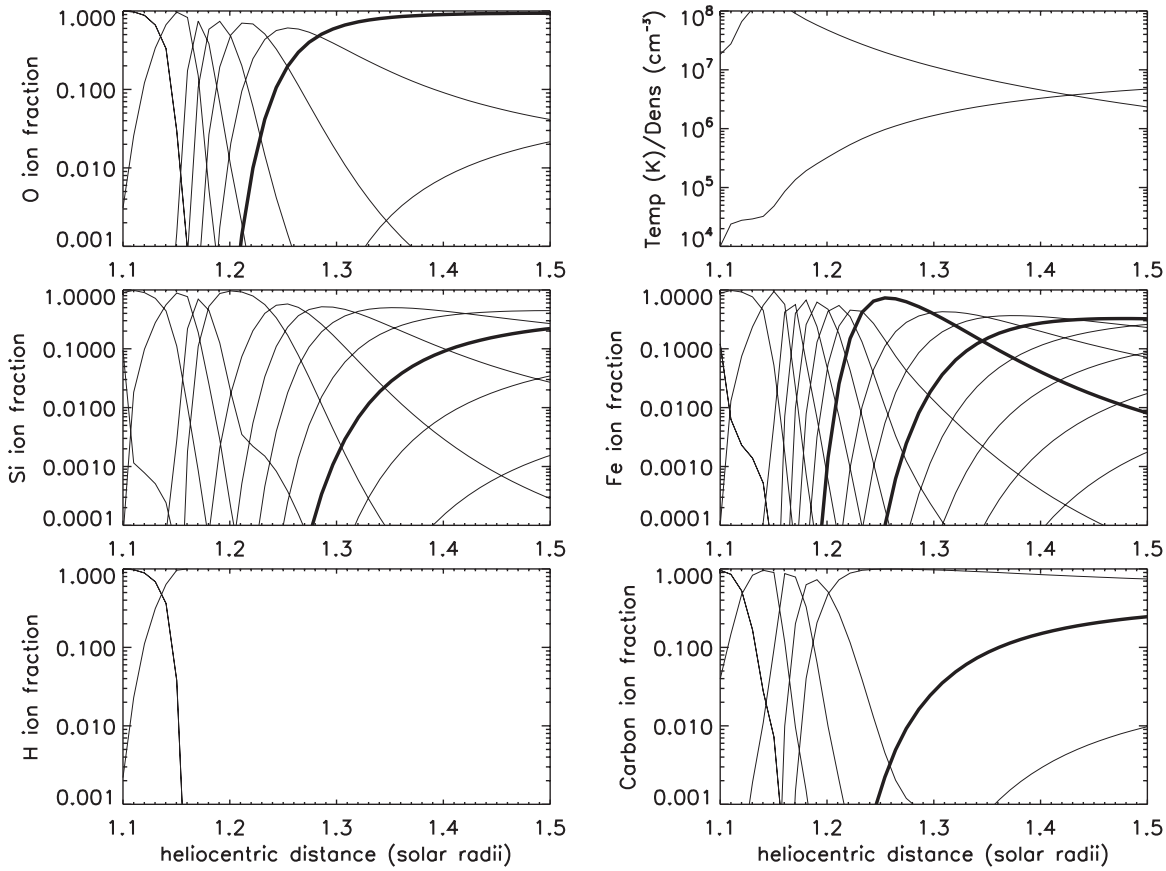

Figure 6. Evolution of charge state distributions for the highest anomalous resistivity considered in model 1 for H, C, O, Si, and Fe. Thick lines highlight O^{+6}, Si^{+9}, Fe^{+8}, Fe^{+11}, and C^{+5}.

The above discussion naturally leads us to our second model to determine if spheromak heating starting from temperatures seen in EUV observations can explain the in situ charge states. In model 2, we started the plasma at 10^6 K, 10^9 cm^{-3}, and a velocity of 100 km s^{-1} similar to the velocity of the filament from Liewer et al. (2009) allowing it to then accelerate to the coasting velocity of 500 km s^{-1}. Starting from this high temperature, the additional heating of the spheromak has no noticeable effect on the charge states. While the temperature was chosen such that the charge states at low heights match observations, the final Fe charge states fall short of those detected in situ. We also experimented with starting at 10^6 K but the higher density and/or at a slower velocity. However, radiative recombination dominated bringing the charge states and temperature rapidly back to their 10^4 K levels. This has implications for the rapidity and amount of energy that had to be dumped into the filaments to produce their high charge states. A thorough examination of this phenomenology is warranted but we leave this to future work. Overall, starting from a higher initial temperature in a uniformly filled spheromak did not solve the problem of matching the highest Fe charge states.

6. DISCUSSION AND CONCLUSIONS

We have explored modeling this filament eruption as due to the heating provided in an expanding spheromak. Figure 6 shows the evolution of H, C, O, Si, and Fe charge states obtained with an anomalous resistivity increased from the classical (i.e., *Spitzer*) value by a factor around 2×10^7–6×10^{11}, as the plasma temperature varies between 10^4 K and 10^7 K. Anomalous resistivity is thought to arise in conditions where plasma turbulence can scatter current carrying electrons and can do so more effectively than the Coulomb collisions between electrons and ions. It may be estimated by replacing the isotropization frequency by Coulomb collisions with the relevant wave–particle interaction rate.

Solutions of the one-dimensional Vlasov equation designed to model the Buneman instability in a reconnecting current sheet (Wu & Huang 2009), and therefore model electrons in Langmuir turbulence, give quiescent values of the anomalous resistivity of $\times 10^7$ the *Spitzer* value, with transient values as high as $\times 10^9$ in a background plasma temperature of 10^7 K. In our case, dropping the anomalous resistivity to $\times 10^{10}$ the classical value, the dominant Fe charge state becomes Fe^{7+}. The ratio of the electron plasma frequency to the collision frequency at 1.4 $R_\odot$ in Figure 6 evaluates to $\sim 10^9$, and probably represents the maximum enhancement in resistivity than one may reasonably expect. Lin et al. (2007) estimate a much higher resistivity from the observed width of current sheets trailing CMEs, as high as 10^{12} times the classical resistivity. Bemporad (2008) revisits this and argues that what is observed as a macroscopic current sheet is in fact an assembly of microscopic current sheets, each with width corresponding to anomalous resistivities similar to those given by Wu & Huang (2009), although possibly attributed to different modes of turbulence. We therefore conclude that magnetic energy dissipated in the expansion of a spheromak may account for the filament heating between 10^4 K and 10^6 K, but is unlikely to be the explanation for the high Fe charge states characteristic of temperatures of order 10^7 K and higher. The nature of the heating specified in the spheromak

solution is such that the heating rate due to anomalous resistivity cannot be increased without limit, even if an anomalous resistivity as high as allowed by the solution could be justified physically.

Higher charge states, beyond Fe^{13+}, must therefore result from other means of heating. Noting that in the 2007 May 19 CME, the highest Fe charge states are observed exterior to the flux ropes, we speculate that reconnection associated with the eruption is most likely. Type II and Type III radio bursts were observed during this eruption (Kerdraon et al. 2010) at times when the CME shock was between 1.2 and 1.4 $R_\odot$ heliocentric distance (Veronig et al. 2008). Bearing in mind that the plasma we observe and model will be at lower altitude than the CME shock, this corresponds very well to the epochs of heating shown in Figure 6. Recent results suggest that reconnection might be an efficient means of heating electrons (Drake et al. 2006; Oka et al. 2010).

In earlier work (Rakowski et al. 2007), we expressed the heat input to the CME in terms of its kinetic energy input by relating the heating to the acceleration, tacitly assuming that the mechanism of acceleration inevitably also supplies heat to the CME plasma. In the case of the spheromak, the heating is related to the expansion, but not the acceleration, so the ratio of heat to kinetic energy does not have a natural interpretation. We estimate it, though, to facilitate comparison with Rakowski et al. (2007). From Equations (11) and (12)

$$\frac{\int \dot{\epsilon} dt}{mv^2/2} = \frac{0.033 B_0^2 R^3 \ln(R/R_0)}{2\pi\rho R^3 v^2/3} = 0.2 \frac{v_A^2}{v^2} \ln\left(\frac{R}{R_0}\right), \quad (18)$$

which close to the Sun evaluates to $\sim$1. This is similar to, but slightly lower than, typical values found by Rakowski et al. (2007). The CMEs studied in that work frequently had charge states of Fe up to neon-like, rather higher than in the flux rope studied here which appear to be consistent with our estimate of thermal to kinetic energy in the CME.

This work has been supported by NASA Contract NNG08EK62I and by basic research funds of the Office of Naval Research.

REFERENCES

Akmal, A., Raymond, J. C., Vourlidas, A., Thompson, B., Ciaravella, A., Ko, Y.-K., Uzzo, M., & Wu, R. 2001, ApJ, 553, 922
Antiochos, S. K., DeVore, C. R., & Klimchuk, J. A. 1999, ApJ, 510, 485
Bemporad, A. 2008, ApJ, 689, 572
Bone, L. A., van Driel-Gesztelyi, L., Culhane, J. L., Aulanier, G., & Liewer, P. 2009, Sol. Phys., 259, 31
Bryans, P., Badnell, N. R., Gorczyca, T. W., Laming, J. M., Mitthumsiri, W., & Savin, D. W. 2006, ApJS, 167, 343
Chandrasekhar, S., & Kendall, P. C. 1957, ApJ, 126, 457
Ciaravella, A., Raymond, J. C., Reale, F., Strachan, L., & Peres, G. 2001, ApJ, 557, 351
Drake, J. F., Swisdak, M., Che, H., & Shay, M. A. 2006, Nature, 433, 553
Fan, Y., & Gibson, S. E. 2004, ApJ, 609, 1123
Gloeckler, G., et al. 1998, Space Sci. Rev., 86, 497
Gopalswamy, N., et al. 2009, ApJ, 691, L123
Henke, T., Woch, J., Schwenn, R., Mall, U., Gloeckler, G., von Steiger, R., Forsyth, R. J., & Balogh, A. 2001, J. Geophys. Res., 106, 10597
Henke, T., et al. 1998, Geophys. Res. Lett., 25, 3465
Kataoka, R., Ebisuzaki, T., Kusano, K., Shiota, D., Inoue, S., Yamamoto, T. T., & Tokumaru, M. 2009, J. Geophys. Res., 114, A10102
Kerdraon, A., Pick, M., Hoang, S., Wang, Y.-M., & Haggerty, D. 2010, ApJ, 715, 468
Kilpua, E. K. J., et al. 2009, Sol. Phys., 254, 325
Kumar, A., & Rust, D. M. 1996, J. Geophys. Res., 101, 15667
Laming, J. M., & Grun, J. 2002, Phys. Rev. Lett., 89, 125002
Laming, J. M., & Grun, J. 2003, Phys. Plasmas, 10, 1614
Laming, J. M., & Hwang, U. 2003, ApJ, 597, 347
Lee, J.-Y., Raymond, J. C., Ko, Y.-K., & Kim, K.-S. 2009, ApJ, 692, 1271
Lepri, S. T., & Zurbuchen, T. H. 2004, J. Geophys. Res., 109, A1112
Lepri, S. T., Zurbuchen, T. H., Fisk, L. A., Richardson, I. G., Cane, H. V., & Gloeckler, G. 2001, J. Geophys. Res., 106, 29231
Li, Y., Lynch, B. J., Stenborg, G., Luhmann, J. G., Huttunen, K. E. J., Welsch, B. T., Liewer, P. C., & Vourlidas, A. 2008, ApJ, 681, L37
Liewer, P. C., de Jong, E. M., Hall, J. R., Howard, R. A., Thompson, W. T., Culhane, J. L., Bone, L., & van Driel-Gesztelyi, L. 2009, Sol. Phys., 256, 57
Lin, J., Ko, Y.-K., Sui, L., Raymond, J. C., Stenborg, G. A., Jiang, Y., Zhao, S., & Mancuso, S. 2005, ApJ, 622, 1251
Lin, J., Li, J., Forbes, T. G., Ko, Y.-K., Raymond, J. C., & Vourlidas, A. 2007, ApJ, 658, L123
Linker, J. A., Mikić, Z., Lionello, R., Riley, P., Amari, T., & Odstrcil, D. 2003, Phys. Plasmas, 10, 1971
Liu, Y., Luhmann, J. G., Huttunen, K. E. J., Lin, R. P., Bale, S. D., Russell, C. T., & Galvin, A. B. 2008, ApJ, 677, L133
Lynch, B. J., Antiochos, S. K., MacNeice, P. J., Zurbuchen, T. H., & Fisk, L. A. 2004, ApJ, 617, 589
Lynch, B. J., Zurbuchen, T. H., Fisk, L. A., & Antiochos, S. K. 2003, J. Geophys. Res., 108, 1239
Lyutikov, M., & Gourgouliatos, K. N. 2010, Sol. Phys., submitted (arXiv: 1009.3463)
Magara, T., & Longcope, D. W. 2003, ApJ, 586, 630
Moore, R. L., Sterling, A. C., Hudson, H. S., & Lemen, J. R. 2001, ApJ, 552, 833
Nakagawa, T., & Matsuoka, A. 2010, J. Geophys. Res., 115, A10113
Oka, M., Phan, T.-D., Krucker, S., Fujimoto, M., & Shinohara, I. 2010, ApJ, 714, 915
Rakowski, C. E., Laming, J. M., & Lepri, S. T. 2007, ApJ, 667, 602
Sui, L., & Holman, G. D. 2003, ApJ, 596, L251
Sui, L., Holman, G. D., White, S. M., & Zhang, J. 2005, ApJ, 633, 1175
Summers, H. P., & McWhirter, R. W. P. 1979, J. Phys. B., 12, 2387
Veronig, A. M., Temmer, M., & Vršnak, B. 2008, ApJ, 681, L113
Wu, G. P., & Huang, G. L. 2009, A&A, 502, 341
Zhang, J., & Dere, K. P. 2006, ApJ, 649, 1100
Zhang, J., Dere, K. P., Howard, R. A., Kundu, M. R., & White, S. M. 2001, ApJ, 559, 452
Zhang, J., Dere, K. P., Howard, R. A., & Vourlidas, A. 2004, ApJ, 604, 420
Zurbuchen, T. H., Gloeckler, G., Ipavich, F., Raines, J., Smith, C. W., & Fisk, L. A. 2004, Geophys. Res. Lett., 31, 11805
Zurbuchen, T. H., & Richardson, I. G. 2006, Space Sci. Rev., 123, 31